Energy Conversion and Management 327 (2025) 119572

Contents lists available at ScienceDirect

Energy Conversion and Management

journal homepage: www.elsevier.com/locate/enconman

Novel concepts for metal hydride storage tanks – Numerical modeling, simulation and evaluation

Chris Drawer [a,*], Lars Baetcke [b], Jelto Lange [a], Yuanyuan Shang [c], Martin Kaltschmitt [a]

[a] Institute of Environmental Technology and Energy Economics (IUE), Hamburg University of Technology (TUHH), Eissendorfer Strasse 40, Hamburg 21073 Germany
[b] Institute of Maritime Energy Systems, German Aerospace Center (DLR), Dünebergerstraße 108, Geesthacht 21502 Germany
[c] Institute of Hydrogen Technology, Helmholtz-Zentrum hereon GmbH, Max-Planck-Straße 1, Geesthacht 21502 Germany

ARTICLE INFO

Keywords:
Finite element method
Metal hydride construction concepts
Hydrogen
Absorption reaction
Reactive hydride composite
Iron titanium

ABSTRACT

The efficient, space-saving and safe storage of hydrogen is a major challenge that needs to be overcome for enabling renewable energy systems. Metal hydrides are a possible solution. But the key challenge is the identification and development of the most promising metal hydride material as well as the ideal tank design for an efficient hydrogen absorption / desorption in terms of energy demand / storage losses and loading / unloading time. Against this background this paper aims to identify suitable combinations of medium and low-temperature metal hydride materials in combination with three different tank design concepts. The goal is to determine which material fits best for each combination and could thus be a suitable solution for a future implementation in stationary and mobile applications of metal hydride storage tanks. To achieve this goal a finite element method (FEM) modeling and simulation of materials and construction designs in COMSOL Multiphysics is realized. The results are analyzed in terms of hydrogen absorption rate, temperature profile over time, and the necessary energy demand for the overall storage process. The results show that for the low-temperature metal hydride investigated here, the tank design is of subordinate importance, allowing for more application-specific design. For medium-temperature metal hydrides, the investigated construction concepts show heterogeneous results. For fast hydrogen absorption and minimal external heating time, the suggested rectangular tank design might be a promising option, requiring only 28% / 29% of the heating energy of the cylindrical concepts. If the goal is to achieve the most complete hydrogen absorption, the base design concept investigated here, consisting of a cylindrical tank with metal hydride material rolled up in a spiral, is the most favorable solution; achieving a hydrogen loading of about 3.6 wt–% for the medium-temperature metal hydride. The low-temperature metal hydride achieves a total hydrogen absorption of around 1.4 wt-% in the optimum concept. For concepts with higher operating temperatures, preheating the storage tank before feeding in the hydrogen could improve the absorption process (only examined here).

1. Introduction and background

The use of “green” hydrogen plays a crucial role within the global defossilization efforts to face climate change. In addition to the challenging production of “green” hydrogen based on renewable sources of energy, a particular challenge lies in the safe, space-saving and energy-efficient storage of hydrogen. “Conventional” forms of hydrogen storage, such as pressurized storage or liquid storage, have the disadvantage that the hydrogen must be kept at high pressure (usually between 200 and 750 bar) or at a very low temperature (−253 °C) for the entire storage period. In addition, hydrogen losses occur during these storage processes [1,2].

Storing hydrogen in the form of metal hydrides is a promising alternative to these conventional storage technologies and offers some notable advantages. Firstly, apart from the loading and unloading processes, the hydrogen is stored under ambient conditions, which simplifies operation [3]. Furthermore, no losses occur during storage as the hydrogen is firmly bound in the material [4]. In addition, hydrogen storage in metal hydrides is characterized by a high volumetric energy density, which – depending on the material used – can in some cases significantly exceed the values of conventional forms of storage [3].

Nevertheless, challenges to be overcome for a large-scale use of the

* Corresponding author.
E-mail address: chris.drawer@tuhh.de (C. Drawer).

https://doi.org/10.1016/j.enconman.2025.119572
Received 12 September 2024; Received in revised form 22 January 2025; Accepted 22 January 2025
Available online 31 January 2025

metal hydride-based storage technology lie in the production of high-performance storage materials as well as in the development of appropriate, efficient tank designs that enable rapid loading and unloading. A particular hurdle is the efficient supply and removal of heat, which is necessary for rapid loading and unloading of the storage tank. So far, the research focus regarding the production of high-performance storage materials has been on optimizing conventional metal hydride materials (FeTi, $LaNi_5$, etc.) by adding additives (e.g. using Ti compounds) and/or improving the manufacturing process (e.g., by ball milling to create the largest possible surface area) [4,5]. One example of the effect of additives was identified in a recent study, which demonstrated the potentially positive impact of metal oxides (such as TiO_3) on the hydrogen absorption rate of magnesium hydrides [6]. Another example can be observed in the field of material pretreatment, where a recent study investigated the extent to which different ball milling times influence the absorption performance of FeTi at different temperatures [7]. The focus in the design of hydrogen storage tanks based on metal hydrides has so far been on creating the best possible conditions for loose fillings by means of heat-conducting structures inside and outside the tank in order to ensure even and rapid distribution / removal of thermal energy necessary for an efficient loading and unloading [8]. Various active and passive thermal management systems have also been investigated recently. For example, it has been investigated how different concepts of internal fin structures in a storage tank affect the optimization of heat distribution and hydrogen flow within the tank [9]. Active heat management methods have also been studied in detail recently, to show the difference between air and water cooling and forced and free convection [10]. In addition, more novel studies also deal with the active internal cooling of metal hydride tanks, as in [11], which generally improve the absorption performance, but are associated with potentially high design costs.

In summary, current and past research primarily focuses on three key areas: optimizing material processing techniques, improving the composition of specific metal hydride materials, and designing, often complex, tank systems, which are typically analyzed using only a selected metal hydride material. Moreover, metal hydride storage tanks have so far largely been developed and modeled for loose fillings of metal hydrides.

However, the focus of the work to date on analyzing only selected metal hydrides and in some cases only one tank concept with slight changes, e.g., to the heat management systems, means that only limited conclusions can be drawn about the use of other materials in these tank concepts.

This research gap is to be closed by addressing both the selection of suitable tank concepts for specific applications (e.g. specific possibilities in the stationary and transport sectors) and by simultaneously analyzing different storage materials that are used within these concepts and are designed for very different properties (low- and medium-temperature metal hydrides).

Within this overall context the aim of this paper is to determine optimal combinations of tank design and storage materials and the associated selected technical parameters as well as to analyze these design-material-combinations with regard to possible applications for metal hydride storage systems. As storage materials, a conventional intermetallic metal hydride material (FeTi) is analyzed and a promising reactive hydride composite (RHC) for hydrogen storage. In addition, the metal hydride materials analyzed in this work are not integrated into the tank concepts as loose bulk materials, as is usually the case, but are bound in a polymer. This ensures on the one hand that no potentially degrading substances (such as oxygen) reach the metal hydride and on the other hand ensures that the metal hydride particles are kept in a confined space [12–14]. This makes it possible to develop completely new, innovative tank concepts in this work.

To investigate these concepts, finite element method (FEM) models of various tank designs and material combinations are created and the absorption process is simulated. The simulation can then be used to compare the various tank designs, including the materials used, on the basis of the technical parameters of hydrogen absorption, the temperature distribution in the tank and the energy requirement of the tank's external heating system, and to determine the optimum tank/material combination in terms of the most energy-efficient and fastest possible hydrogen absorption performance.

These results can contribute to better mapping the speed and completeness of hydrogen absorption in the context of larger energy system analyses and thus improve the informative value of such energy systems.

2. Methodological approach

The objective is to investigate the performance of different tank design concepts and different metal hydride materials for the determination of the best combinations. The different construction variants (designs) and materials as well as the simulation of hydrogen absorption are based on the given physical–chemical relationships (software COMSOL Multiphysics) on the basis of measurements on the materials and an existing work. In that work, a comprehensive modeling, simulation and evaluation of a novel design variant of a metal hydride storage tank and an innovative reactive hydride composite was carried out [13]. The tank design developed therein, a cylindrical tank with a spiral-shaped metal hydride coil (design 1) with the used metal hydride (material 1), was designed in the course of that work with a focus on an optimum heat distribution. This solution will therefore serve as a base case within this paper.

Building on this, two novel tank construction variants and one additional, commercially available metal hydride material is added to the assessment and shall be characterized and analyzed in detail in this work. The choice of two very different metal hydrides, which cover, more or less, two ends of the metal hydride storage technology, should allow a good assessment of a later potential application-related use.

Since the basic modeling strategy is to be kept simple, it is assumed that the hydrogen is initially fed in at ambient conditions (1 bar, 25 °C) and that the tank is also at ambient conditions when the storage reaction starts. The heating of the tank required for the RHC is to be provided by an external electrical heating jacket.

In particular, the procedure according to [13] will be used for modeling the reaction kinetics and the heat integration. Experimental reaction kinetics data for both investigated materials are available and used to define the simulation parameters. In parallel, different construction design concepts are developed. Every design concept and every material are combined and one absorption cycle is simulated.

The results are compared with each other and are analyzed in terms of hydrogen absorption (time and mass), temperature distribution within the storage tank and necessary external energy demand for heating the reactor.

The procedure is shown in Fig. 1.

3. Definition of designs

Three different design concepts for metal hydride storage systems will be examined. These are based on some key aspects that are decisive for the design of metal hydride storage systems and in particular for storage systems with the materials used here.

- The thickness of the solid metal hydride composites (metal hydride material combined with the polymer) have to be smaller than 2 mm (no inhibition by diffusion) [15].
- For modeling purposes, the need for fluid mechanical simulations should be avoided, which was ensured in this work by the implementation of permeable grid structures and a central hydrogen supply for an unimpeded flow of hydrogen [13].
- New manufacturing processes based on commercially available variants are to be included.

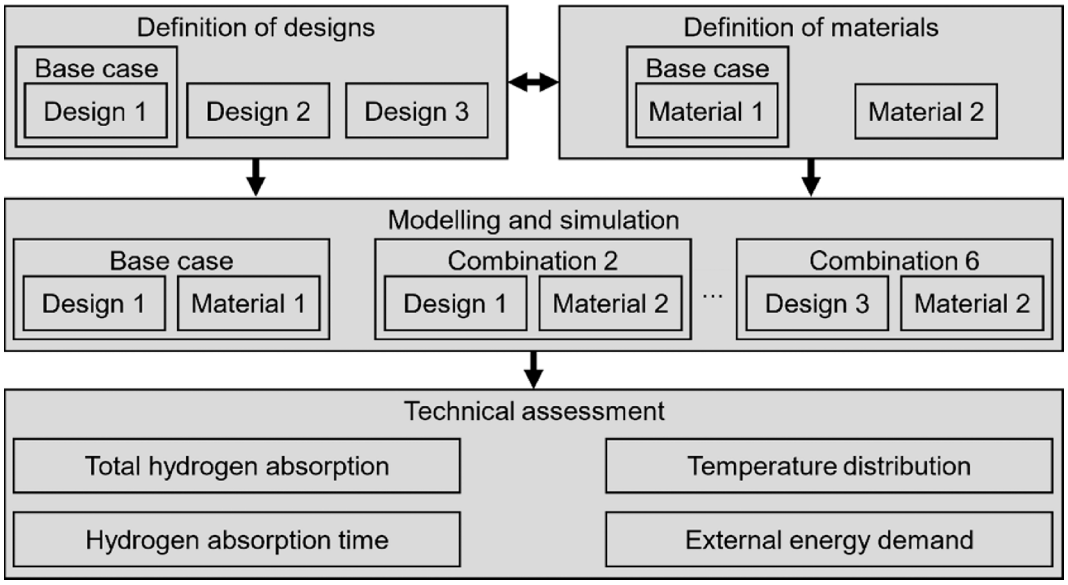

Fig. 1. Procedure.

All designs have the same diameter (cylinder) / the same edge lengths (rectangle) inside and outside the tank, the same length and the same size of the outer heating jacket including the insulation [13].

3.1. *Design concept 1 – Coiled construction in radial direction*

The first concept developed in [13] is a storage tank with new innovative material. This made it necessary to develop a small foil of polymethylpentene combined with the RHC which ensures that the diffusion of hydrogen, which has to pass the polymer, does not affect the chemical reaction with the metal hydride (chapter 4). Also, no filter is required between the hydrogen stream and the metal hydride, since with the polymer unnecessary oxygen contamination is avoided. In addition, fast thermal management had to be ensured.

The solution is therefore to roll up the metal hydride composite material alternately with a metal with high thermal conductivity designed as a grid structure. Various reinforcing thermal management systems were analyzed with the result that radial, narrow rips, which also consist of a grid-shaped, highly conductive metal, represent the optimum design for this construction [13]. The design analyzed here shown in Fig. 2.

3.2. *Design concept 2 – Cylindrical, layered construction in axial direction*

With a potentially higher proportion of metal hydride material (> 50 %) within the polymer matrix, the production of a film is more limited. And, a metal grid structure in design concept 1 resulted in very even heat distribution inside the tank [13]. A direct connection from the outer shell to the inside of the storage tank might be even more advantageous

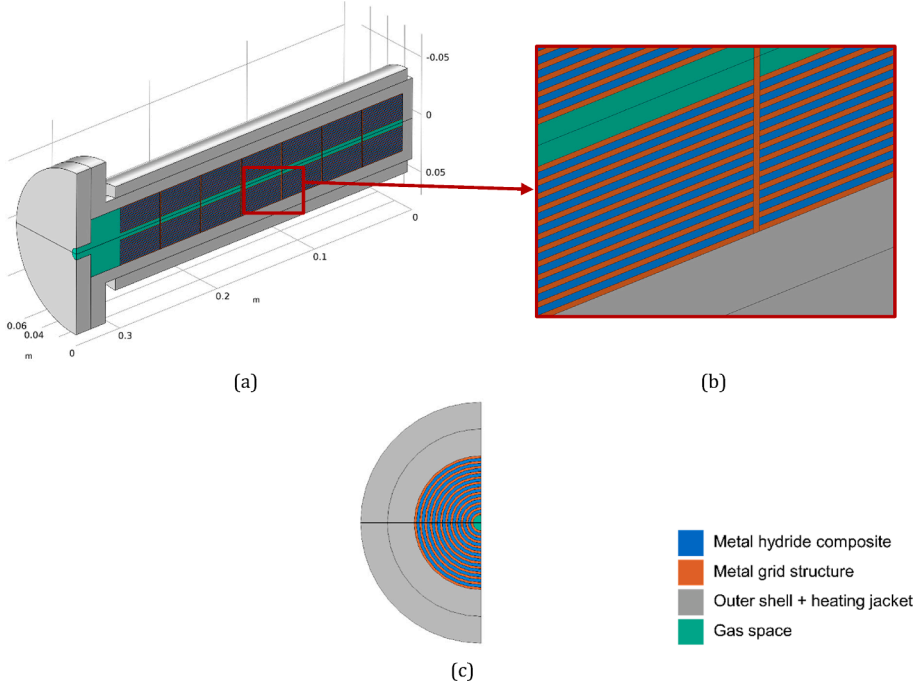

Fig. 2. Coiled construction in radial direction (a), developed by [13]. Magnification of an area (b).

in terms of heat conduction.

Commercially available innovative concepts for metal hydride storage tanks use metal hydride material pressed into round disks and combined into a cylinder of the desired length [16]. This enables more scaling options for metal hydride storage materials and, additionally, no filter between hydrogen and metal hydride is necessary.

This leads to the concept of small metal hydride disks, separated from small grid structures. This enables to conduct the thermal energy which has to be transferred from the outer shell of a hydrogen storage tank into the center of the tank. Grid structures ensure an unhindered hydrogen flow, additionally to a central hydrogen supply. This design concept is shown in Fig. 3.

3.3. Design concept 3 – Rectangular, layered construction

A disadvantage of the second concept is that the production of round disks implies considerable production losses (the disks need be punched out during manufacturing) to be recycled. Such material losses can be avoided / minimized by using rectangular plates made of metal hydride composite material containing metal hydride and polymer.

Therefore, as a further option, a rectangular tank design is investigated combining an easy construction concept from the second concept, with the manufacturing possibility of punching out the material within the production concept and the alternating grid structure / metal hydride polymer in radial direction from the first base concept. For enhancing the share of active material inside the tank, no central hydrogen supply is assumed but the grid structure in the middle is designed slightly thicker than the other layers for enhanced permeability.

Typically, sharp edges in a rectangular tank might result in temperature hot spots. Furthermore, sharp edges in pressurized tanks might lead to enhanced structural stress [17]. To avoid these problems, the rectangular tank was modelled with rounded edges inside the storage tank (a comparison of sharp edges with rounded edges is shown in the supplementary material, chapter 1). The optimized grid structure from concept 1 is also assumed for enhanced heat distribution inside the storage tank. This construction design is shown in Fig. 4.

4. Definition of storage materials

In the following, the characteristic specifications of the metal hydride storage materials selected for this work and a polymer as an auxiliary material are outlined.

4.1. Storage materials

Many different materials can be used for hydrogen storage using metal hydride technology. These various materials / material combinations differ quite a lot in terms of storage capacities, temperature levels, etc. [3]. From this wide variety, one example of a reactive hydride composite and one example of an intermetallic hydride are evaluated. The reason for the selection is that two metal hydrides with properties as different as possible should be chosen in order to investigate the applicability of the developed tank models not only for one class of metal hydrides, but to cover as wide a range as possible. In addition to the gravimetric energy density, which differs significantly for the two metal hydrides listed here, significantly different temperature levels are of particular relevance for the suitability of the tank models. Additionally, a polymer material is used intended to protect the metal hydride materials from contamination by impurities in the hydrogen stream or by components from the atmosphere (e.g., oxygen) and to keep the metal hydride particles in a confined space for optimization of the hydrogen cycling process.

4.1.1. Complex metal hydride – 6 $Mg(NH_2)_2$-9LiH-$LiBH_4$ (RHC)

Complex metal hydrides are characterized by high volumetric energy densities (up to 91 kg_{H2}/m^3; $LiBH_4$) and high theoretical storage capacities (up to 18.5 wt-%; $LiBH_4$) [3,4]. Operating temperatures are in the range of 500 to 1,000 °C with operating pressures between 1 and 200 bar [3,4]. Mainly due of this high temperature level, complex metal hydrides are not yet in the broad focus for practical applications [3].

These drawbacks can be overcome by combining different complex metal hydrides. The resulting combinations, called reactive hydride composites (RHC), show lower storage capacities but also lower temperature levels which make them more interesting for practical applications.

One example is the material 6 $Mg(NH_2)_2$-9LiH-$LiBH_4$ [14]. This metal hydride is characterized by a theoretical hydrogen storage capacity of 4.3 wt-%; experiments have shown a reversible hydrogen uptake of up to 3.8 wt-% [14]. Experimental investigations show that average conditions in terms of temperature (180 °C) and pressure (50 to 80 bar) are sufficient for the desired absorption reaction [13,14]. For the sake of simplicity, the term “RHC” will be used for 6 $Mg(NH_2)_2$-9LiH-$LiBH_4$.

Improvements in terms of reduction of temperature and pressure level can be achieved by implementing different additives (e.g. [14]) in the RHC. But this will not be considered further in the remainder of this paper due to the lack of data.

4.1.2. Intermetallic metal hydride – Iron titanium

Iron titanium (FeTi) is a common material for metal hydride storage systems in terms of low-temperature metal hydrides. Compared to RHC described above, FeTi has a storage capacity in terms of hydrogen absorption at 1.9 wt-% in theory. Experiments have shown a reversible

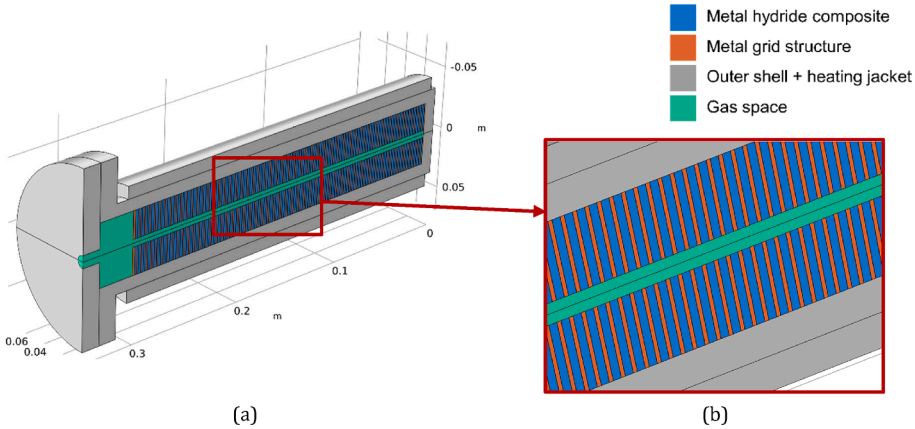

Fig. 3. Cylindrical, layered construction in axial direction (a), magnification of an area (b).

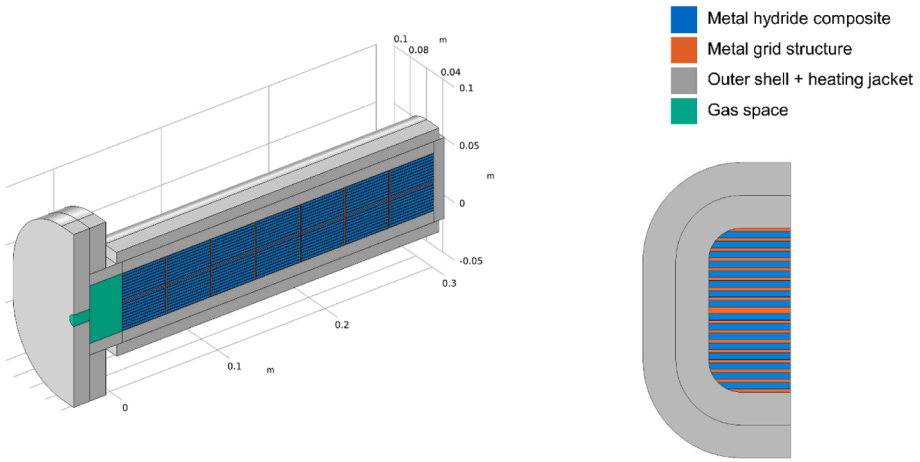

Fig. 4. Rectangular, layered construction (a), cut through the tank (b).

storage capacity of around 1.37 wt-% at a pressure of 65 bar and a temperature of 40 °C [18]. These near-ambient temperature makes FeTi a promising candidate for low-temperature application cases for hydrogen storage in the stationary and transportation sector (e.g. [3]). The material is already used in small scale applications, developed by the company GKN Hydrogen [19].

4.2. Polymer material

RHC is very sensitive to impurities (e.g., oxygen) possibly contained within the hydrogen stream and/or coming from the atmosphere [20]. This is the reason why the material is embedded (for all designs, described in chapter 3) in a polymer to maintain cycle stability and to confine the metal hydride to improve the cycling process [12]. It was shown that polymethylpentene (poly(4-methyl-1-pentene; commercially available as TPX™) is suitable for this task [20,21]. Therefore, the metal hydride materials assessed here are mixed with polymethylpentene in a proportion of 50 % metal hydride material and 50 % polymethylpentene by volume [4]. Higher shares of metal hydride material as active material for absorption might be possible but if the contamination barrier works undisturbed with lower shares of polymer material is not investigated so far.

5. Modelling and simulation

In the following, the developed models are described. This includes the assumptions, the different reaction kinetics for the various storage materials, the heat integration and the hydrogen inflow, distribution and diffusion into the material.

Typically, decisive effects occur either during absorption or desorption; i.e., it is usually sufficient to consider one of the two partial reactions. In particular, heat management plays a greater role during the storage process of hydrogen in complex metal hydrides (such as the used RHC). If absorption is optimized in terms of rate, rapid desorption can also be assumed [13]. For intermetallic, low-temperature metal hydrides (FeTi), a less comprehensive heat management is necessary and it can therefore be considered sufficient to consider only the absorption. For these reasons, only the absorption process is described here.

5.1. Assumptions

The model of a metal hydride storage tank is realized by a multi-physical concept with a combination of.

- implementation reaction kinetics of metal hydride materials,
- integration of heat (supplied from external heating and from the metal hydride material itself) and
- hydrogen distribution in the storage tank via diffusion.

To make the model run with these complex working concepts, assumptions have to be made, mainly to ensure proper simulation time. Some of the most important assumptions, including key boundary and initial conditions, are briefly explained below.

1) Mechanical stress at the outer shell is neglected; it is assumed that the thickness of the wall is sufficient to avoid mechanical damage in all cases.
2) Metal hydride material expands when hydrogen is absorbed [22]. This expansion is neglected, whereby the available gas room at the beginning of the storage process ensures that the material can expand in the horizontal direction without disrupting the hydrogen flow. The integrated polymer also provides a certain stability and helps the storage material to expand; these measures can prevent vertical expansion and thus damage to the tank walls [23].
3) No fluid mechanics module is implemented in the model. The selection of the grid structure with a high porosity, an empty gas room at the lower end of the tank and (for some models) the hydrogen supply through the center of the tank is assumed to ensure an even hydrogen distribution within the overall tank.
4) The pressure which is applied at the reaction is assumed to be constant ($p_R = const.$) throughout the tank and over the entire absorption time.
5) The porosity of the composite and the respective active materials are assumed to be uniform throughout the overall tank.
6) Local thermal equilibrium is assumed for the fluid (hydrogen) and the solid material.
7) No hydrogen passes from the inside of the tank to the outside through the tank walls, i.e., a no flux condition is assumed.

8) A convection term was implemented on the outer shell or at points where the heating jacket rests, whereby free convection with external temperature $T_{ext} = T_{environment} = 25^{\circ} C$ is assumed.
9) Diffusion takes place inside the tank exclusively of hydrogen in the direction of the composite; other diffusions, e.g., out of the material, are assumed to be zero.
10) As part of the tank modeling, both the 2D models (design concept 1 and 2) and the 3D model (design concept 3) were assumed to be (axially) symmetrical through the middle of the tank.

5.2. Reaction kinetics

In the following, the reaction kinetics for both assesses metal hydride materials (i.e., FeTi and RHC) is described. Since the validation for the RHC used was described in detail in [13], the reaction kinetics will only be briefly discussed. The reaction kinetics for FeTi are explained in detail.

5.2.1. Iron titanium

The chemical reaction for the hydrogenation of iron titanium is shown in Eq. (5–1).

$$FeTi + H_2 \rightleftharpoons FeTiH_2 \tag{5.1}$$

Initially, the maximum theoretical hydrogen storage capacity ($w_{H2,max}$) must be calculated as shown in Eq. (5–2). This can be realized with the molar mass of hydrogen (M_{H2}) divided by the sum of the molar mass of hydrogen and iron titanium (M_{FeTi}) [24,25].

$$w_{H2,\max,FeTi} = \frac{100 M_{H2}}{M_{H2} + M_{FeTi}} = 1.9\, wt - \% \tag{5.2}$$

For the determination of the hydrogen inlet concentration at the beginning of the absorption, a procedure in accordance with [13] is realized.

The concentration of the entire reaction mixture can be calculated by dividing the density of the hydrogenated iron titanium (ρ_{FeTiH2}) by the molar masses of hydrogen and iron titanium as well as through the number of moles of iron titanium through the total mol number being 1/2. It is assumed that, in analogy to the RHC, half of the material is polymethylpentene and half of the material is metal hydride. Furthermore, the hydrogen is by stoichiometry half of the reaction components. This results in the necessary inlet concentration of hydrogen ($c_{0,H2}$) (Eq. (5–3)).

$$c_{0,H2} = \frac{1}{2}\frac{1}{2}\frac{\rho_{FeTiH2}}{\frac{1}{2}(M_{H2} + M_{FeTi})} = 27,874 mol \Big/ m^3 \tag{5.3}$$

For validation, the reaction rate of the measured hydrogen storage capacity is determined. The difference is calculated from experimental data using 5 s intervals. It is assumed, that within the 5 s intervals the reaction rate is constant. Afterwards, the reaction rate is implemented in the simulation model. The hydrogen absorption of the experimental data is shown in Fig. 5.

Eq. (5–4) applies for the determination of the reaction kinetics [26]. The change of reacted metal hydride over time $\left(\frac{dc_{FeTiH2}}{dt}\right)$ can be expressed by the reaction rate in dependence of temperature, pressure and time ($r(T,p,t)$) multiplied with the starting concentration of the metal hydride iron titanium ($c_{0,FeTi}$).

$$\frac{dc_{FeTiH2}}{dt} = r(T,p,t) c_{0,FeTi} \tag{5.4}$$

For the determination of the reaction rate, the formulation from [26] was used. The reaction rate depends on the points outlined below.

- The temperature is implemented with the Arrhenius expression ($k_{Arr}(T)$, Eq. (5–5)), with the pre-exponential factor (A), the activation energy (E_a), the general gas constant (R) and the temperature (T).

$$k_{Arr}(T) = A e^{\frac{-Ea}{RT}} \tag{5.5}$$

- The pressure is applied via the driving force (f_{force}, Eq. (5–6)) consisting of the reaction pressure (p_R) and the equilibrium pressure ($p_{eq}(T)$).

$$f_{force} = \ln\left(\frac{p_R}{p_{eq}(T)}\right) \tag{5.6}$$

According to [26], the equilibrium pressure for the absorption reaction can be determined given the known reaction enthalpy (ΔH_R), reaction entropy (ΔS_R) and ambient pressure (p_0) (Eq. (5–7)).

$$p_{eq}(T) = e^{\frac{\Delta H_R}{RT} - \frac{\Delta S_R}{R}} p_0 \tag{5.7}$$

- The reacted share (X) of metal hydride over time is expressed via the model from Johnson-Mehl-Avrami (JMA, dimensional factor n = 1) ($g(X)$, Eq. (5–8)) [18]. The reacted share can be expressed by the reacted metal hydride over time ($c_{FeTiH2}(t)$) divided by the initial metal hydride material ($c_{0,FeTi}$).

$$g(X) = (1 - X) \tag{5.8}$$

This results in Eq. (5–9) for the overall reaction rate.

$$r(T,p,t) = A e^{\frac{-E_a}{RT}} \ln\left(\frac{p_R}{p_{eq}(T)}\right)\left(1 - \frac{c_{FeTiH2}(t)}{c_{0,FeTi}}\right) \tag{5.9}$$

In addition to the general equation, some adjustments to the developed reaction kinetics are required.

With a storage capacity of 1.37 wt-%, only 72 % of the theoretical load of 1.9 wt–% could be achieved in experimental tests. This results in the factor 0.72 in the denominator of the JMA-model. For general flattening of the determined reaction kinetics, the factor 0.98 is added to the expression of the reaction rate and the logarithmic progression is achieved by changing the expression $c_{0,FeTi}$ from Eq. (5–4) to

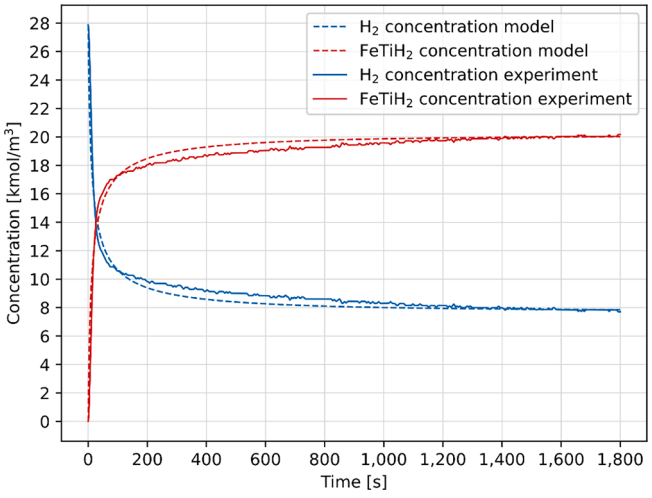

Fig. 5. Comparison of developed reaction kinetics and experimental data from [18] for hydrogen absorption.

Table 1
Parameters for developing reaction kinetics of hydrogenating FeTi.

Parameter	Symbol	Value	Reference
Activation energy	$E_{a,FeTiH2}$	39,288 J/mol	calculation
Ambient pressure	p_a	1.013 bar	assumption
Ambient temperature	T_a	25 °C	assumption
Density iron titanium	ρ_{FeTi}	6.79 g/cm^3	[18]
Density iron titanium hydride	ρ_{FeTiH2}	5.90 g/cm^3	[24]
Maximum theoretical hydrogen storage capacity	$w_{H2,max,FeTiH2}$	1.9 wt-%	calculation
Molar mass hydrogen	M_{H2}	2.106 g/mol	[25]
Molar mass iron titanium	M_{FeTi}	103.727 g/mol	[24]
Molar mass polymethylpentene	M_{TPX}	84.16 g/mol	[27]
Pre-exponential factor	A_{FeTiH2}	184.241 ·10^3 1/s	calculation
Reaction enthalpy for formation of $FeTiH_2$	$\Delta H_{R,FeTiH2}$	−24,600 J/mol	[18]
Reaction entropy for formation of $FeTiH_2$	$\Delta S_{R,FeTiH2}$	−100.8 J/(mol K)	[18]
Reaction pressure experiment	p_R	65 bar	[18]
Reaction rate constant at 65 bar and 40 °C	K	0.0515 1/s	[18]
Reaction temperature experiment	T_R	40 °C	[18]
Starting concentration iron titanium	$c_{0,FeTi}$	27,874 mol/m^3	calculation

$c_{\mathrm{FeTi}}(t) - 0.24c_{0,FeTi}$. These two factors were determined empirically and iteratively. As a control instance within the simulation, the equation was multiplied by the time-dependent development of the hydrogen loading of the tank.

Table 1 summarizes all data which is used to develop the reaction kinetics.

The final reaction kinetics for iron titanium is shown in Eq. (5–10).

$$\frac{dc_{FeTiH2}}{dt} = 0.98A_{FeTi}e^{\frac{-E_{a,FeTi}}{RT}}\ln\left(\frac{p_R}{p_{eq}(T)}\right)\left(1-\frac{c_{FeTiH2}(t)}{0.72c_{0,FeTi}}\right)(c_{\mathrm{FeTi}}(t)-0.24c_{0,FeTi})\frac{c(t)_{H2}}{c_{0,H2}} \tag{5.10}$$

The results of the comparison of the developed reaction kinetics with the experimental data for hydrogen absorption from [18] are shown in Fig. 5. Here it can be seen that the experimental data can be adequately expressed by the equation developed. The largest deviation is observed 5 s after the start of the reaction, where the calculated concentration of the remaining hydrogen is higher than the experimental analysis. After 30 s, the concentration of the remaining hydrogen is 8 % higher compared to the experimental data. The average deviation is 3 %. Detailed data for validation and plausibility tests (e.g., the pressure and temperature dependence) can be found in the supplementary material, chapter 2.

5.2.2. 6 $Mg(NH_2)_2$-9LiH-$LiBH_4$

A reaction kinetic for RHC used here was developed by [13] with data from [14] and is shown in Eq. (5–11) till (5–13). Similar to the reaction kinetics of iron–titanium, the equation consists of the temperature-dependent Arrhenius expression and the pressure-dependent driving force. It also contains an empirically determined pre-factor and the damping functions D and U, which are dependent on the concentration of lithium borohydride amide at the start of the reaction ($c_{Li_4BH_4(NH_2)_3,0}$) and during the reaction ($c_{Li_4BH_4(NH_2)_3}$).

Table 2
Parameters for developing reaction kinetics of hydrogenating the investigated RHC.

Parameter	Symbol	Value	Reference
Activation energy	$E_{a,RHC}$	136,000 J/mol	[13]
Pre-exponential factor	A_{RHC}	9.64 ·10^{14} 1/s	[13]
Maximum theoretical hydrogen storage capacity	$w_{H2,max,RHC}$	4.2 wt-%	[13]
Starting concentration RHC	$c_{0,RHC}$	18,461 mol/m^3	[13]

$$r\left(\frac{dc_{RHC}}{dt}\right) = 0.72Ae^{\frac{-E_a}{RT}}\ln\left(\frac{p_R}{p_{eq}(T)}\right)D\left(c_{Li_4BH_4(NH_2)_3}\right)U\left(c_{Li_4BH_4(NH_2)_3}\right) \tag{5.11}$$

$$D = c_{Li_4BH_4(NH_2)_3,0} - 0.89c_{Li_4BH_4(NH_2)_3} \tag{5.12}$$

$$U = c_{Li_4BH_4(NH_2)_3} - 0.18c_{Li_4BH_4(NH_2)_3,0} \tag{5.13}$$

Some selected parameters for the RHC reaction kinetic are summarized in Table 2. As with FeTi, the initial concentration of hydrogen for the stoichiometric reaction is based on the assumption that polymethylpentene and RHC are present in a 50 % mixture by volume (for deeper insights into details of the developed reaction kinetics see [13]).

5.3. Heat integration

Heat is formed / released during loading / unloading of the metal hydride. Furthermore, to overcome the activation energy of the absorption process and to ensure an ongoing reaction, even when the temperature falls below the necessary value for the activation energy, additional heat may be supplied.

As a result of [13], an electric heating jacket is used to heat the storage tank from outside. This technical solution enables flexible temperature control, which is not the case with liquid heating being a possible alternative.

The heating balance can be described with Eq. (5–14) as the sum of supplied heat from the used heating jacket ($\dot{Q}_{heating}$), the heat supplied by the reaction ($\dot{Q}_{reaction}$), and the heat lost by natural convection ($\dot{Q}_{natcon}$) outside of the storage tank [13].

$$0 = \dot{Q}_{heating} + \dot{Q}_{reaction} - \dot{Q}_{natcon} \tag{5.14}$$

The heating jacket can be controlled via a factor (X) multiplied by the heating power of the jacket ($P_{heating}$) (Eq. (5–15)) [13].

$$\dot{Q}_{heating} = XP_{heating} \tag{5.15}$$

The heat supplied by the absorption reaction can be described via Eq. (5–16) consisting of the reaction kinetic expression $r\left(\frac{dc_{MH}}{dt}\right)$ multiplied with the reaction enthalpy of the absorption reaction for forming the metal hydride ($\Delta H_{R,MH}$) [9].

$$\dot{Q}_{reaction} = \frac{dc_{MH}}{dt}\Delta H_{R,MH} \tag{5.16}$$

The natural convection can be expressed by Eq. (5–17) with the heat transfer coefficient (α), the outside surface of the storage tank (A) and the temperature difference from the tank wall and the surrounding environment ($|T_{wall} - T_{amb}|$).

$$\dot{Q}_{natcon} = \alpha A|T_{wall} - T_{amb}| \tag{5.17}$$

The heat capacity ($c_{p,TPX}$) for polymethylpentene known and can be assumed to be constant [13,28]. The combined heat capacity of polymethylpentene-RHC with a 50 % admixture of TPX is known from [13]. There are various empirical equations to describe the heat capacity of iron titanium. For reasons of simplification and because the temperature range investigated here is relatively small, a constant value for the heat capacity is assumed [29]. To combine the heat capacities (c_P) of the mixture for polymethylpentene-FeTi, the Neumann-Kopp additive rule is applied, using the molar masses of the polymethylpentene (M_{TPX}) and the metal hydride material (M_{FeTi}) and the respective heat capacities ($c_{P,FeTi}$ and $c_{p,TPX}$) [30]. The combined heat capacity is calculated using Eq. (5–18). The specific heat capacity of polymethylpentene clearly exceeds that of FeTi, although the focus of the combined specific heat capacity is on the side of FeTi due to a higher molar mass [28,29].

$$c_p = \frac{M_{FeTi}c_{P,FeTi} + M_{TPX}c_{p,TPX}}{M_{FeTi} + M_{TPX}} \tag{5.18}$$

The thermal conductivity of the mixtures (λ) relevant for the thermal conduction within the materials is determined by the idea of the parallel mixing concept. The combined thermal conductivity of polymethylpentene-RHC with a 50 % admixture of TPX is known from [13]. The volumetric proportions of polymethylpentene (ϕ_{TPX}) and FeTi (ϕ_{FeTi}) and their assumed constant thermal conductivity (λ_{TPX} and λ_{FeTi}) are used to calculate the mixture conductivity of polymethylpentene-FeTi [31]. The thermal conductivity of FeTi significantly exceeds that of polymethylpentene [28,32]. The resulting, combined thermal conductivity is shown in Eq. (5–19).

$$\lambda = \phi_{TPX}\lambda_{TPX} + \phi_{FeTi}\lambda_{FeTi} \tag{5.19}$$

5.4. Hydrogen transport

The hydrogen is assumed to be evenly distributed within the tank. At the beginning of the storage process, the respective hydrogen inflow is modeled for an ideal reaction with iron titanium and the RHC at the beginning of the storage tank. Afterwards the hydrogen is first distributed within the gas room and diffuses through the composite of iron titanium and polymethylpentene / RHC and polymethylpentene. For unimpeded hydrogen flow through the grid structures to ensure a good contact with hydrogen and active material and for a good heat conduction through the tank, the porosity of the grid structure is assumed to be 0.6 chosen based on the results of [13]. The transport of hydrogen through the active material is assumed to be diffusion-based.

To ensure an efficient simulation, the concept of a “Thin Diffusion Barrier” was implemented into the model. This makes it possible to define diffusion on boundaries without necessarily refining the grid structure within the FEM (finite element method) environment [33]. This is implemented with the use of Fick’s first law (Eq. (5–20)) [34]. The diffusional flux (J) can be described by the diffusion coefficient (D) multiplied with the concentration gradient $\left(\frac{dc}{dx}\right)$.

$$J = -D\left(\frac{dc}{dx}\right) \tag{5.20}$$

The layer thickness (d_{Diff}) for the assumed diffusion barrier can be implemented as follows, whereby the concentration gradient (Δc) describes the concentration difference between inside and outside the material. The adapted equation is shown in Eq. (5–21).

$$J = -D\frac{\Delta c}{d_{Diff}} \tag{5.21}$$

For the RHC, the thickness of the layer was set to $5{\cdot}10^{-7}$ m and showed no changes in the behavior of the absorption reaction when set to smaller or higher values. Pre-investigations have shown that for FeTi the layer thickness plays a major role in determining the time required for the hydrogen to be fully absorbed in the metal hydride material. It is not possible to estimate with certainty which thickness of the thin diffusion barrier comes closest to reality. Therefore, a conservative value of 2 mm is assumed for the thickness of the metal hydride composite itself. Thinner layer lead to faster hydrogen absorption; examples which show the start of the absorption process are shown in the supplementary material, chapter 3.

The diffusion coefficient for hydrogen was set to $2.07{\cdot}10^{-9}$ m^2/s [13].

6. Technical assessment

The results of the different construction concepts and the corresponding metal hydride materials are presented below. Here, the material results will be compared for each construction concept individually. The focus is on analyzing the following key parameters.

- Hydrogen absorption in mass percent of absorbed hydrogen depending on the time course of the absorption reaction at different points inside the tank.
- Overall hydrogen absorption in mass percent of absorbed hydrogen in the entire tank depending on the time course of the absorption reaction and the volumetric energy density in mass absorbed hydrogen per volume.
- Temperature development as a function of time of the absorption reaction at different points in the tank.
- The required thermal energy to be supplied by means of the external heating jacket, mapped by switching on or off, depending on a certain average temperature on the inside of the tank.

6.1. Hydrogen absorption

The aim is to achieve a hydrogen absorption as fast as possible; i.e., a rapidly rising curve at the start of the loading process. The respective hydrogen absorbed in the metal to form metal hydrides is given below.

6.1.1. Design concept 1

Fig. 6 shows the measurement points in the construction design according to [13]. The concept is axisymmetric which makes it sufficient to use this 2D (two-dimensional) view for hydrogen absorption. The results of the hydrogen absorption generated with data from [13] are shown in Fig. 7.

RHC. The absorption reaction at the B- and C-points starts after roughly 500 s (Fig. 7 (a)), proceeds rapidly and is already completed after around 100 s. At the A-points near the inlet of the storage tank, the start of the reaction is delayed by several hundred seconds and is only completed at the outermost points after the simulated absorption time has elapsed after 2,500 s. This effect is related to the temperature distribution in the tank (chapter 6.2).

FeTi. The results for the combination of design concept 1 and the material FeTi is shown in Fig. 7 (b). Here the reaction starts immediately after the start of the hydrogen influx. This can be explained by the fact that the absorption reaction already starts at room temperature (25 °C). The reaction is fast and completed in all observed measurement points after about 400 s, including all A-points; i.e., the simulation is

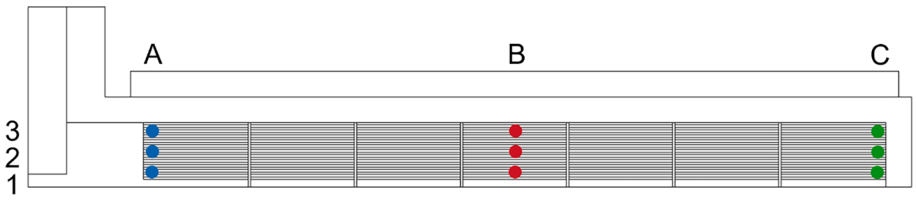

Fig. 6. Design concept 1 with measurement points, generated with data from [13].

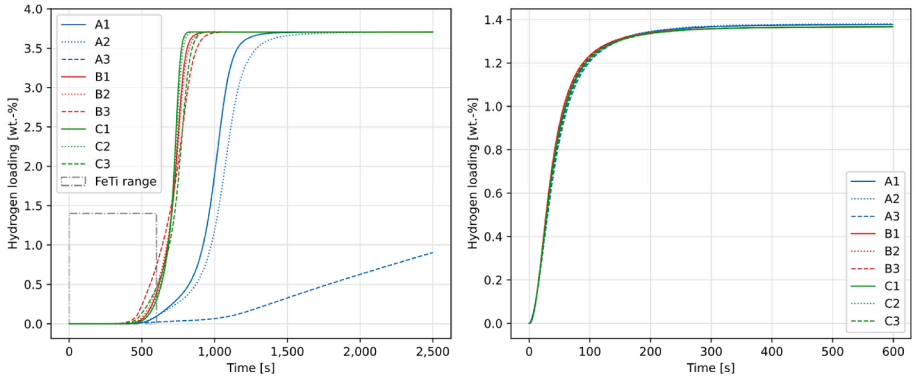

(a) (b)

Fig. 7. Hydrogen absorption within design concept 1, for RHC (data used according to [13]) (a) and for FeTi (b).

completed after 600 s. For a better comparison with the material RHC, the considered range for FeTi is marked in Fig. 7 (a). This is also continued in the following diagrams.

6.1.2. *Design concept 2*

The measurement points for the design concept 2 is shown in Fig. 8. Analog to design concept 1 (chapter 3.1), the concept is axisymmetric and thus the observation of a 2D model is sufficient. All measurement points are located in the middle of a metal hydride composite disk.

RHC. The results for implementing the RHC material in design concept 2 are shown in Fig. 9 (a). The absorption reaction in the center of the storage tank (B-points) begins a few moments before the 500 s mark is reached and proceeds very quickly until 700 s, where the reaction is complete. The reaction at the end of the storage tank (C-points) starts a few seconds later. This reaction is initially less rapid than in the middle of the tank but after a few moments the reaction proceeds also very fast and ends at about 1,000 s. A significant difference to concept 1 are the A-points, at which the reaction cannot be started during the entire simulation time because the required temperature level is not reached (chapter 6.2). One solution could be to preheat the storage tank

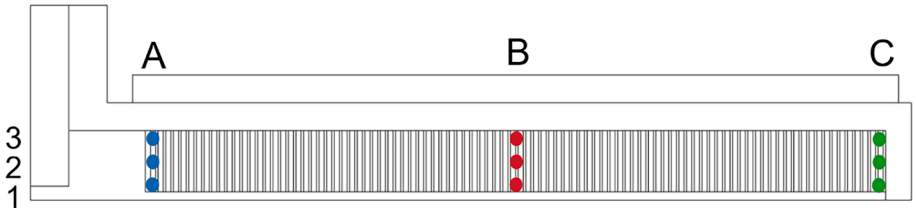

Fig. 8. Design concept 2 with measurement points.

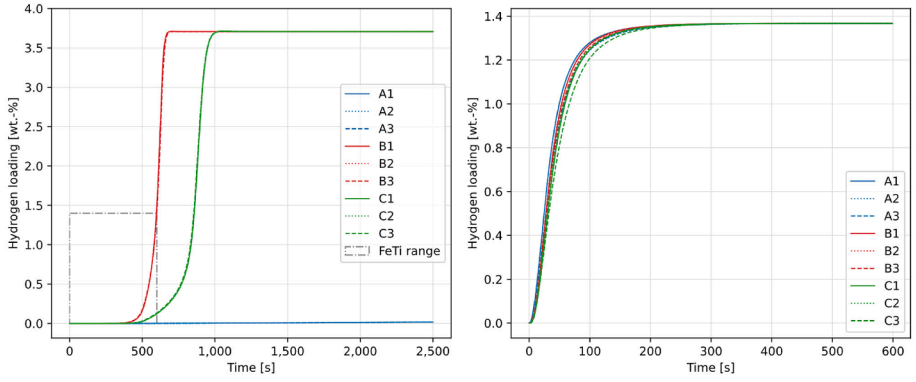

(a) (b)

Fig. 9. Hydrogen absorption within design concept 2, for RHC (a) and for FeTi (b).

(supplementary material, chapter 4). Furthermore, it can be observed that all B-points and C-points show the same absorption performance, so that no difference can be seen between the points further inside and those further outside the storage tank. This can be attributed to the very uniform heat distribution by means of the direct connection via the grid structures from the inside of the tank to the center of the tank, which ensures uniformly good hydrogen absorption.

FeTi. Fig. 9 (b) shows the results for the combination of design concept 2 and FeTi. In analogy to design concept 1 with FeTi, the reaction starts immediately after the hydrogen flows inside the tank. There is no significant difference whether the measurement points are at the beginning or at the end of the storage tank or are more inside or more outside. The reaction is finished after around 200 s being even faster than for concept 1 with FeTi. One reason may be the 22 % larger metal hydride surface area of design concept 2 compared to design concept 1, which might enable a faster diffusion of hydrogen into the material.

6.1.3. Design concept 3

For the results of design concept 3 additional measurement points are necessary because this model is not axisymmetric and needs to be analyzed in 3D (three-dimensional). The measurement points of design concepts 1 and 2 have been extended by 9 additional points one level lower (D, E, F) and three further points (X, Y, Z) in the rounded corners (Fig. 10).

In order to keep the presentation of the results comprehensible, the hydrogen absorption results were divided into two diagrams for the RHC (Fig. 11 (a) and (b)) and for FeTi (Fig. 11 (c) and (d)).

RHC. The results of the combination of concept 3 with the RHC are similar to the results of concept 1; absorption starts first at the B-points, then at the C-points and significantly later at the A-points. In contrast to concept 1, however, the first hydrogen absorption begins after 150 s, which is much faster. This can be explained by the direct contact of all grid structures with the tank wall, which thus ensures good heat distribution within the storage tank (chapter 6.2.3). The absorption performance of the A-points is worse than in concept 1, in which at least the measurement points further inwards have completely finished the absorption cycle. Although the tank is not axisymmetric, there appears to be little difference between the measurement points in Fig. 11 (a) and (b) demonstrating a uniform hydrogen distribution even at the outer points of the tank. In comparison to concept 2, concept 3 is characterized by two differently aligned heat conducting structures, which lead both as rips from the inside of the tank wall to the middle of the tank, as well as grid structures as plates, which lead from the hydrogen inlet to the end of the tank. This difference seems to favor the faster hydrogen absorption in a direct comparison of concept 2 and 3.

FeTi. Fig. 11 (c) and (d) show the results for the combination of design concept 3 and FeTi. There is only a small difference in hydrogen absorption between points A and C (Fig. 11 (c)) and D to Z (Fig. 11 (d)); this is similar to the results of the RHC. Furthermore, the rectangular design shows the slowest hydrogen absorption in comparison to the absorption performance of design 1 and 2 for FeTi, with a completed absorption cycle after around 600 s. Nevertheless, in direct comparison to the RHC, the hydrogen is completely absorbed within the simulated time.

6.1.4. Overall hydrogen absorption

In order to analyze the completeness of the absorption not only for the individual selected points, but also for the entire tank, the time-varying hydrogen absorption in the entire tank is also specified below. The indication in weight-percentage makes it possible to visualize the difference to the real storage capacities measured in the tank.

The overall hydrogen absorption within the storage tank concepts in weight-percentage can be seen in Fig. 12 (a) for RHC and in Fig. 12 (b) for FeTi.

Looking at the concepts with RHC included, the highest share of hydrogen being within the storage tank at the end of the simulation can be seen for the base case (design 1) from [13]; this option shows also the slowest absorption time. Design concept 2 is characterized by a faster hydrogen uptake but reaches a lower total hydrogen content at the end of the simulation. The fast uptake mainly results from the structure of metal hydride disks, alternating with metal grid structures. The fastest absorption can be observed in the rectangular concept 3, which starts much earlier compared to the other concepts, presumably as a result of the better heat distribution, but takes longer to reach full hydrogen loading, which is not achieved at the end of the simulation. In direct comparison to concept 1, this is due to the lower absorption rate in the A-points. This in turn can be explained by the insufficient temperature level of concept 3 in the A-points (chapter 6.2.3).

The opposite picture emerges for the FeTi contained in the concepts in Fig. 12 (b), where concept 3 has the slowest overall hydrogen absorption time, followed by very similar hydrogen loading behavior of concept 1 and 2.

Based on the maximum stored hydrogen at the end of the simulation times (Fig. 12), the porosity of the storage composite of 0.1, the densities of the various storage and polymer materials, the volumetric energy density can be determined in relation to the proportion of storage material in the various concepts. The energy densities are shown in Table 3. The volumetric energy densities are significantly lower compared with those from the literature (e.g. [3]), as the 50 % proportion of the polymer in terms of volume reduces the actual values. Furthermore, it can be

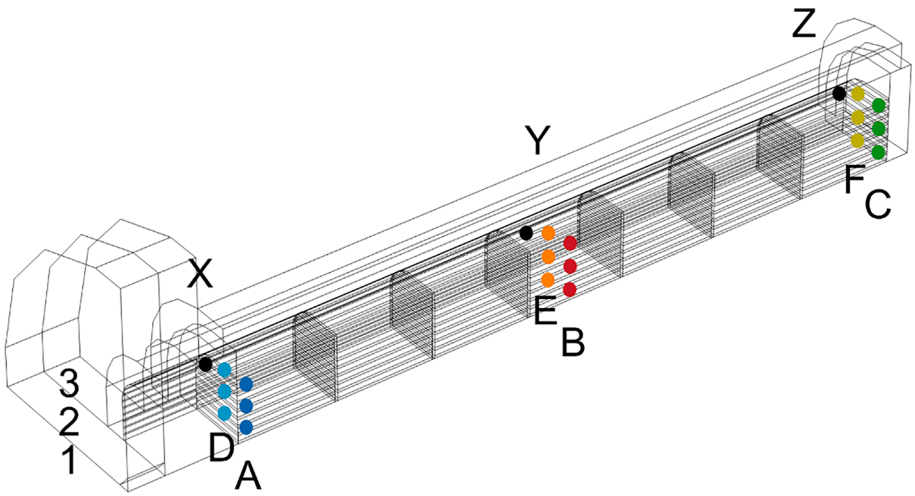

Fig. 10. Design concept 3 with measurement points.

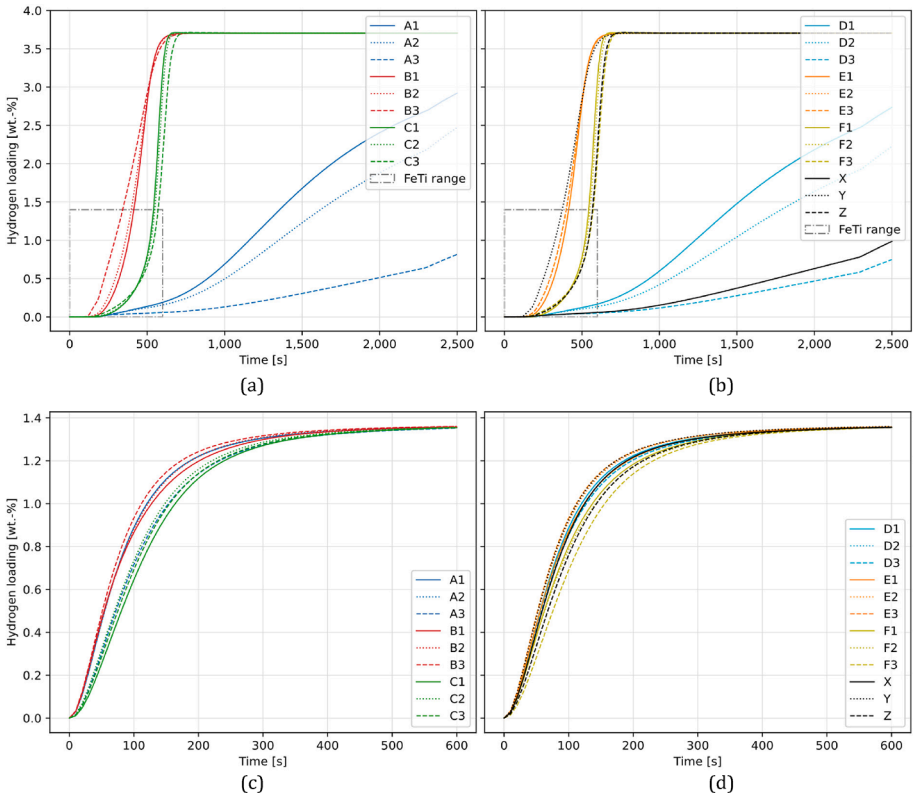

Fig. 11. Hydrogen absorption within design concept 3, RHC measurement points A, B, C (a) and D, E, F, X, Y, Z (b) and FeTi measurement points A, B, C (c) and D, E, F, X, Y, Z (d).

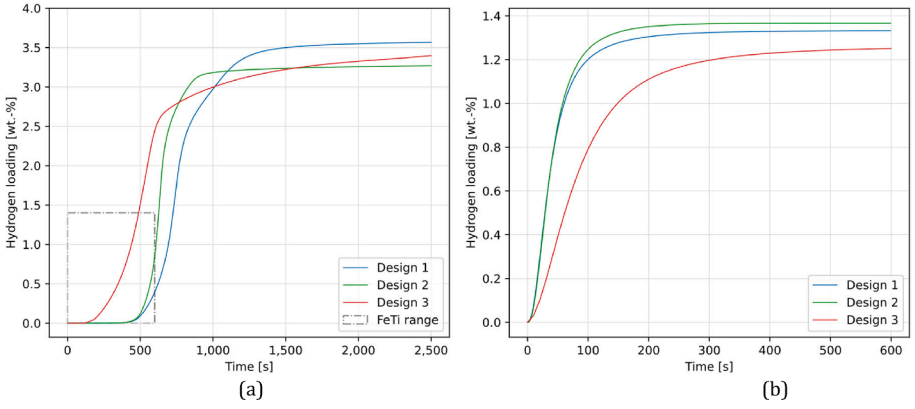

Fig. 12. Overall hydrogen loading for all design concepts, with RHC (a) and FeTi (b).

Table 3
Volumetric energy densities of different design concepts and different metal hydrides.

Design concept	Share of composite[a] [%]	Volumetric energy density – Material[b] [kg_{H2}/m^3]		Volumetric energy density – System[c] [kg_{H2}/m^3]	
		RHC	FeTi	RHC	FeTi
Design 1	48	21.1	39.7	10.1	19.1
Design 2	59	19.3	42.8	11.4	25.2
Design 3	57	19.9	39.7	11.3	22.6

[a] Combination of metal hydride and polymethylpentene.
[b] Based on the composite.
[c] Based on the available system room inside the storage tank.

seen that design concept 2 has the highest composite content and consequently the highest volumetric energy density in relation to the system. As expected, the volumetric energy density of the intermetallic metal hydride FeTi is higher than that of the complex reactive hydride composite.

6.2. *Temperature distribution*

Knowledge of the temperature curves is of great importance both for heating the storage tank in the case of RHC material and for potential utilization of the “excess” heat from the storage tank. For the same measurement points as shown in chapter 6.1, the results for the temperature distribution for all concepts and materials are shown below.

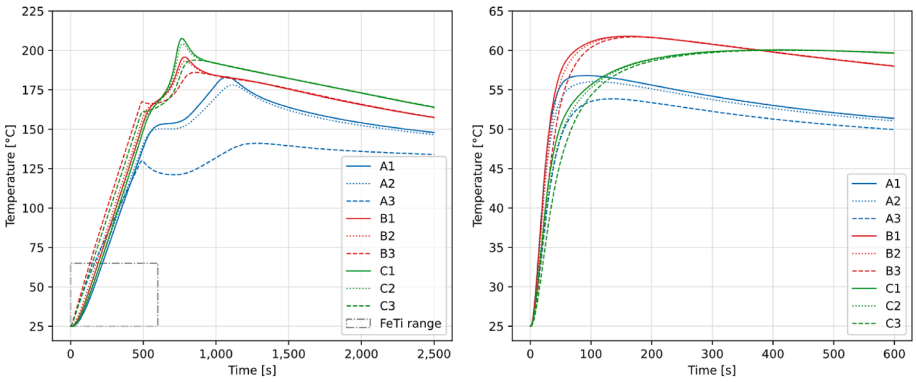

Fig. 13. Temperature distribution within design concept 1, for RHC (data used according to [13]) (a) and for FeTi (b).

6.2.1. Design concept 1

The temperature distribution for design concept 1 and the RHC and FeTi is shown in Fig. 13.

RHC. At the beginning of the process, the storage tank is heated up via the electrical heating jacket (chapter 6.3). At about 500 s, the temperature is high enough to start the reaction and the reaction generates enough heat to sustain itself (Fig. 13 (a)). This leads to a temperature peak at point C1 after around 750 s at 208 °C. Afterwards the temperature is constantly decreasing. Points A1 and A2 reach their temperature peak around 400 s later explaining the slower hydrogen absorption observed in Fig. 7. Point A3 does not reach a temperature high enough to ensure complete absorption of the hydrogen until the end of the simulated time span. This can be explained by the fact that both the hydrogen to be introduced and the tank are at ambient temperature at the start of the loading process. The heating jacket cannot heat the tank at the inlet to the temperature required for the reaction.

FeTi. The temperature distribution for design concept 1 in combination with FeTi can be seen in Fig. 13 (b). No heating for the metal hydride is necessary and the temperature rises rapidly up to 62 °C in point B1 after 160 s. The other B-points are very similar while the point A1 reaches only 57 °C after 85 s. In contrast to the design concept with RHC, the C-points reach their maximum after the A- and B-points at 60 °C after 350 s. In addition, the temperature curves for FeTi are significantly flatter compared to the RHC.

6.2.2. Design concept 2

The temperature profile for the combination of design concept 1 and the RHC and FeTi is shown in Fig. 14.

RHC. Similar to design concept 1 with the RHC, the temperature rises constantly in all B-points (temperature peak at 219 °C after 650 s) and all C-points (temperature peak at 197 °C after 950 s) (Fig. 14 (a)). The highest temperature within the simulation is around 10 K higher compared to design concept 1. The A-points show much lower temperature peak (104 °C after 515 s); they do not reach the necessary temperature for the absorption reaction. This explains why no hydrogen is absorbed at all at these points.

FeTi. Fig. 14 (b) shows the temperature profile for the FeTi material. The curves look very similar to design concept 1 but with a higher overall temperature peak at 71 °C after 200 s being around 10 K higher compared to design concept 1. In contrast to the concept with the RHC, the A-points heat up rapidly, even if they stagnate at a lower temperature level compared to the B- and C-points.

6.2.3. Design concept 3

In addition to the evaluation of the hydrogen absorption results, further measurement points were added for the temperature distribution in comparison to concepts 1 and 2. However, as these are analogous to measuring points A, B and C, similar to hydrogen absorption, the extended points were not shown due to the lack of added value.

RHC. Fig. 15 (a) shows the results for the material RHC. The temperature for the third concept and the RHC material rises rapidly in all points at the start of the absorption process (including external heating of the tank). While the temperature in the B-points and the C-points continues to rise, the temperature of the A-points stagnates after about 250 s at a level between 125 and 150 °C resulting in a lower hydrogen uptake compared to the other measuring points. The overall temperature peak of the measurement points is the same as in construction concept 1 with 208 °C after 610 s. As the heater is switched on again briefly after 2,290 s (due to the reduced average temperature in the tank and the associated instruction to restart it), a slight temperature increase can be seen in Fig. 15 (a). Compared to concept 1, the temperature rises faster leading to a faster hydrogen absorption. On the one hand, the

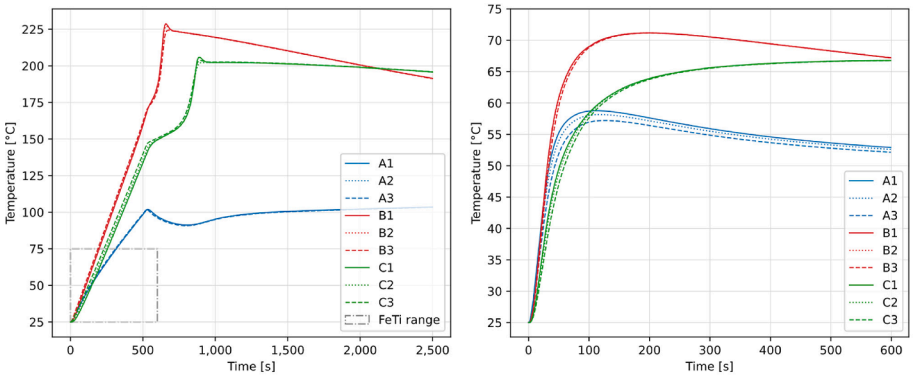

Fig. 14. Temperature distribution within design concept 2, for RHC (a) and for FeTi (b).

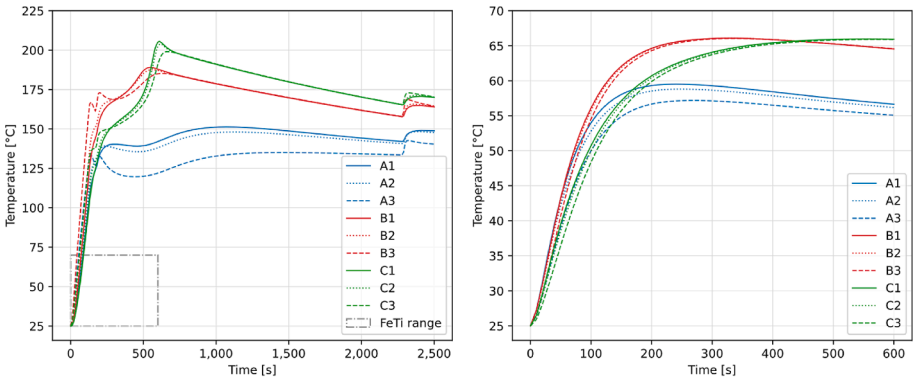

Fig. 15. Temperature distribution within design concept 3, RHC measurement points A, B, C (a) and FeTi measurement points A, B, C (b).

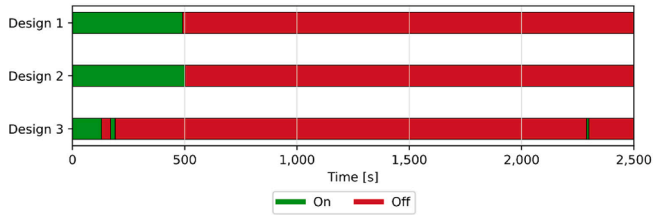

Fig. 16. Heating settings for design concept 1, design concept 2 and design concept 3 with RHC.

good heat-conducting connection of the grid structure (connected to the tank wall) ensures a rapid temperature build-up, but on the other hand, it fails to achieve the required temperature. One possible reason for the somewhat worse hydrogen absorption performance of concept 3 may be the significantly earlier shutdown of the heating compared to concept 1 (Fig. 16). This is controlled by an average temperature to be determined in the entire tank. Although this is high enough across the entire tank, it does not ensure the required increase in temperature at the A-points (at the tank inlet). An improvement can therefore be achieved by turning off the heating later.

FeTi. Compared to construction designs 1 and 2, the temperature profile for concept 3 shows the slowest increase (Fig. 15 (b)). The pattern is similar to the other constructions with FeTi; i.e., the B-points show the highest temperature rise at the beginning and the highest temperature peak, followed by the C-points and the A-points (at a lower level). The overall temperature peak is at 66 °C after 300 s.

6.3. External energy demand

For reaching the reaction temperature of the RHC, the hydrogen storage tank must be heated up. As mentioned at the beginning, an external heating jacket is installed on the outer shell of the storage concepts for this purpose, which is operated electrically. Another option would be an oil-powered liquid heating system, for example. However, firstly, the concept should be kept as simple as possible and secondly, the switch-on/switch-off can be controlled more precisely, although there is always a certain inertia in the system due to the heat capacity present in the tank wall and the grid structure. After the reaction reaches a certain point, it can supply enough heat for itself and the heating jacket is turned off. The switch-off is implemented in the model as an automatic mechanism as soon as a certain average temperature is reached over the entire length of the inner tank wall. Fig. 16 shows, at what time the heating jacket is turned off (and turned on again if necessary) for all three construction concepts with heating (for RHC).

For the first construction concept, heating is turned off after 480 s, followed by design concept 2 19 s later. For both concepts the reaction can supply the heat for the overall remaining time. The third design concept, in which the heating jacket is switched off after just 120 s, shows a different picture. However, unlike the other concepts, the heating needs to be turned on again after 170 s or 2,290 s for 10 s in each case to sustain the absorption reaction.

The outer heating jacket has an output of 1,200 W, from which the energy requirement of the different storage concepts can be determined. Concept 1 requires 160 Wh, concept 2 166 Wh and concept 3 47 Wh, which is significantly less heat.

6.4. Verification of the results

In this chapter, the models and concepts developed in this work will be critically scrutinized, particularly from the point of view of verifying the results generated from them.

The analysis is based on two reaction kinetics of metal hydride materials, one of which is experimentally validated as part of the work of [13] and a second of which is created as part of this work and validated and optimized with experimental data from [18]. The reaction kinetics created in this work was also checked for plausibility by analyzing different pressure and temperature levels.

In contrast, the three tank models are only simulated and due to the lack of real possibilities to carry out experimental analyses on such tanks, a validation is not possible. Nevertheless, by comparing similar simulation-based studies, a certain verification, or at least a plausibility check, can be carried out. Comparisons can only be made with the material FeTi, as there is only one study used in this work for the RHC as a new material, which represents the numerical tank simulation. In addition, all tank models in this work have been newly developed, so that any comparison can only be an approximation and complete comparability is never given.

Selected results that can be compared with other work to a limited extent are the reaction kinetics of FeTi and the general shapes of temperature and hydrogen absorption curves for metal hydride storage tanks (for the use of the material FeTi, or similar intermetallic metal hydride materials).

The reaction kinetics developed in chapter 5.2.1 shows a very fast hydrogen absorption kinetics, where the absorption is already finished after 500 to 600 s. This fast reaction kinetics of FeTi is supported by the work of [26], in which a reaction kinetics was developed for the same material, which ensured an almost complete absorption of hydrogen after about 500 s. The fast reaction kinetics for FeTi can be confirmed by the work of [35]. The general pressure and temperature dependence as well as the fast absorption kinetics can also be supported by the work of [36]. The work of [37] can be used to check the plausibility of the hydrogen absorption of the tank models. In that work, an intermetallic metal hydride material is used, which works at comparable pressures and temperatures to FeTi. The investigated tank is a cylindrical tank. In

the work, both modeling and experiments are carried out, which correspond to the results of this work at pressure and temperature changes. The faster absorption at increasing pressures and the faster absorption at increasing temperatures should be emphasized, which is analogous to the curves of this work (see Suppl material). The sharp rise in temperature at the start of loading can also be observed in this work and in [37], although the temperature in this work drops more slowly due to the insulation of the tank. A similarly fast hydrogen absorption could be shown by the work of [38] using a different intermetallic metal hydride.

In summary, the results of this study are consistent with the results of a limited number of similar studies in the literature and can therefore be considered plausible.

7. Conclusions

The aim of this paper is the technical assessment of various combinations of tank constructions / designs as well as different metal hydride materials by means of an FEM (finite element method) analysis. Aspects of hydrogen absorption and temperature distribution within the storage tanks as well as the externally provided energy demand are analyzed. The key results are summarized and discussed below.

- The highest hydrogen absorption using RHC material is achieved with a cylindrical design with alternating coiled metal hydride and grid spacers (concept 1). A rectangular tank with alternating metal hydride plates and grids (concept 3) absorbs hydrogen fastest locally but takes longer overall than concept 1. The most incomplete absorption occurs in a cylindrical structure with alternating metal hydride disks and grids (concept 2), hindered by poor absorption near the tank inlet.
- In all concepts with the RHC material, hydrogen absorption is significantly better in the middle and end of the tank than near the inlet, due to the “cold” hydrogen at 25 °C. Preheating the tank, as demonstrated for concept 2, improves absorption markedly, especially at temperatures above 100 °C (see supplementary material, chapter 4). While reducing the inlet space could also be beneficial, sufficient expansion volume for the metal hydride must be ensured, though this aspect was not modeled here.
- Potentially suitable design concepts for most transportation applications should be characterized by a fast filling rate for the hydrogen within an acceptable time period [3]. Based on the assumptions and simplifications made here, this applies mainly to the rectangular concept 3 with a RHC showing a fast hydrogen absorption, a potentially simpler packing factor than cylindrical designs and, if preheating is implemented, complete absorption.
- Hydrogen is fully absorbed for FeTi, regardless of the tank concept. This is due to the advantage of FeTi, where absorption is independent of external heat. The prerequisite is the even distribution of hydrogen, which is assumed in all the tank concepts considered. This is particularly advantageous for stationary applications, where a compact tank design may not be as necessary as in transportation applications, and also applies to the gravimetric energy density, which is quite low for FeTi compared to the RHC.

There are points which are not investigated in this work and should be in the focus of further research:

- Preheating, as briefly investigated in this work, could be a way to improve the absorption efficiency for the design variants investigated with RHC. Further research questions could be how this can be implemented as efficiently as possible and what temperature level is preferred.
- The choice of heating technology for high-temperature design concepts remains an open question. Electric heating, used here for its simplicity and precise control, proved sufficient only until the reaction becomes self-sustaining, requiring no further adjustment. Future work should explore integration with larger systems, considering interactions with other heat sources or demands. Overall, these factors must be evaluated within the broader context of integrating metal hydride storage into an overarching energy system.

CRediT authorship contribution statement

Chris Drawer: Writing – original draft, Validation, Software, Methodology, Investigation, Formal analysis, Conceptualization. **Lars Baetcke:** Writing – review & editing, Validation, Software. **Jelto Lange:** Writing – review & editing, Supervision. **Yuanyuan Shang:** Resources, Data curation. **Martin Kaltschmitt:** Writing – review & editing, Supervision, Methodology.

Funding

This work was funded by the German Federal Ministry of Education and Research (BMBF) via the project HyPoKo (Grant no. 03SF0657A-D). Open Access funding enabled and organized by project DEAL.

Declaration of competing interest

The authors declare that they have no known competing financial interests or personal relationships that could have appeared to influence the work reported in this paper.

Appendix A. Supplementary data

Supplementary data to this article can be found online at https://doi.org/10.1016/j.enconman.2025.119572.

Data availability

Data will be made available on request.

References

[1] Elberry AM, Thakur J, Santasalo-Aarnio A, Larmi M. Large-scale compressed hydrogen storage as part of renewable electricity storage systems. Int J Hydrogen Energy 2021;46(29):15671–90. https://doi.org/10.1016/j.ijhydene.2021.02.080.
[2] Mulky L, Srivastava S, Lakshmi T, Sandadi ER, Gour S, Thomas NA, et al. An overview of hydrogen storage technologies – Key challenges and opportunities. Mater Chem Phys 2024;325:129710. https://doi.org/10.1016/j.matchemphys.2024.129710.
[3] Drawer C, Lange J, Kaltschmitt M. Metal hydrides for hydrogen storage – Identification and evaluation of stationary and transportation applications. J Storage Mater 2024;77. https://doi.org/10.1016/j.est.2023.109988.
[4] Klopčič N, Grimmer I, Winkler F, Sartory M, Trattner A. A review on metal hydride materials for hydrogen storage. J Storage Mater 2023;72:108456. https://doi.org/10.1016/j.est.2023.108456.
[5] Nivedhitha KS, Beena T, Banapurmath NR, Umarfarooq MA, Ramasamy V, Soudagar MEM, et al. Advances in hydrogen storage with metal hydrides: Mechanisms, materials, and challenges. Int J Hydrogen Energy 2024;61:1259–73. https://doi.org/10.1016/j.ijhydene.2024.02.335.
[6] Rathi B, Agarwal S, Shrivastava K, Kumar M, Jain A. Recent advances in designing metal oxide-based catalysts to enhance the sorption kinetics of magnesium hydride. Int J Hydrogen Energy 2024;53:131–62. https://doi.org/10.1016/j.ijhydene.2023.12.031.
[7] Baran A, Jensen TR, Polański M. High-temperature high-pressure reactive ball milling synthesis of Mg-Ni-based solid-state hydrogen storage materials. J Storage Mater 2024;103:114271. https://doi.org/10.1016/j.est.2024.114271.
[8] Disli T, Çetinkaya SA, Ezan MA, Colpan CO. Numerical investigations on the absorption of a metal hydride hydrogen storage tank based on various thermal management strategies. Int J Hydrogen Energy 2024;51:504–22. https://doi.org/10.1016/j.ijhydene.2023.07.122.
[9] Liu L, Wang K, Luo H, Lu Z, Ning H, Wang X, et al. Fin structure optimization for improving heat transfer efficiency and hydrogen absorption rate of metal hydride hydrogen storage tank. Int J Hydrogen Energy 2024;65:362–74. https://doi.org/10.1016/j.ijhydene.2024.04.067.
[10] Zhu J, Lin X, Lv L, Li M, Luo Q, Kudiiarov VN, et al. The relationship between thermal management methods and hydrogen storage performance of the metal hydride tank. J Mater Sci Technol 2024;203:66–77. https://doi.org/10.1016/j.jmst.2024.03.018.

[11] Sreeraj R, Aadhithiyan AK, Anbarasu S. Advanced design methodology and modelling of a finned metal hydride reactor using multi-objective Jaya algorithm and desirability approach. J Storage Mater 2024;98:113017. https://doi.org/10.1016/j.est.2024.113017.
[12] Abetz C, Georgopanos P, Pistidda C, Klassen T, Abetz V. Reactive Hydride Composite Confined in a Polymer Matrix: New Insights into the Desorption and Absorption of Hydrogen in a Storage Material with High Cycling Stability. Adv Materials Technologies 2022;7(11):2101584. https://doi.org/10.1002/admt.202101584.
[13] Baetcke L. Wärmemanagementsysteme für Leichtmetallhydrid-Wasserstoffspeicher: Entwicklung, Analyse und Vergleich unter Berücksichtigung der Wasserstoffspeicherdynamik [Dissertation]. Hamburg: Technische Universität Hamburg; 2021.
[14] Cao H, Zhang W, Pistidda C, Puszkiel J, Milanese C, Santoru A, et al. Kinetic alteration of the 6Mg(NH 2) 2 –9LiH–LiBH 4 system by co-adding YCl 3 and Li 3 N. Phys Chem Chem Phys 2017;19(47):32105–15. https://doi.org/10.1039/C7CP06826C.
[15] Weigelt F, Georgopanos P, Shishatskiy S, Filiz V, Brinkmann T, Abetz V. Development and Characterization of Defect-Free Matrimid® Mixed-Matrix Membranes Containing Activated Carbon Particles for Gas Separation. Polymers (Basel) 2018;10(1). https://doi.org/10.3390/polym10010051.
[16] Liu L, Ilyushechkin A, Liang D, Cousins A, Tian W, Chen C, et al. Metal Hydride Composite Structures for Improved Heat Transfer and Stability for Hydrogen Storage and Compression Applications. Inorganics 2023;11(5):181. https://doi.org/10.3390/inorganics11050181.
[17] Lewiński J. The effect of manhole shape and wall thickness on stress state in a cylindrical pressure vessel. jtam 2015:59. doi: 10.15632/jtam-pl.53.1.59.
[18] Shang Y, Liu S, Liang Z, Pyczak F, Lei Z, Heidenreich T, et al. Developing sustainable FeTi alloys for hydrogen storage by recycling. Commun Mater 2022;3(1). https://doi.org/10.1038/s43246-022-00324-5.
[19] GKN Hydrogen. [April 03, 2024]; Available from: https://www.gknhydrogen.com/.
[20] Cao H, Georgopanos P, Capurso G, Pistidda C, Weigelt F, Chaudhary A-L, et al. Air-stable metal hydride-polymer composites of Mg(NH2)2–LiH and TPX™. Mater Today Energy 2018;10:98–107. https://doi.org/10.1016/j.mtener.2018.08.008.
[21] Mitsui Chemicals. TPX. [June 26, 2024]; Available from: https://jp.mitsuichemicals.com/en/special/tpx/.
[22] Cui Y, Zhang Z, Zeng X, Kou H. Numerical analysis of heat and mass transfer during hydrogen absorption in metal hydride beds with a novel peridynamic model. Appl Therm Eng 2022;209:118294. https://doi.org/10.1016/j.applthermaleng.2022.118294.
[23] Yang FS, Wang GX, Zhang ZX, Meng XY, Rudolph V. Design of the metal hydride reactors – A review on the key technical issues. Int J Hydrogen Energy 2010;35(8):3832–40. https://doi.org/10.1016/j.ijhydene.2010.01.053.
[24] Padhee SP, Roy A, Pati S. Mechanistic insights into efficient reversible hydrogen storage in ferrotitanium. Int J Hydrogen Energy 2021;46(1):906–21. https://doi.org/10.1016/j.ijhydene.2020.09.221.
[25] Wiberg E, Wiberg N. Inorganic Chemistry. San Diego, Calif., London: Academic; 2001.
[26] Zeaiter A, Nardin P, Pour Yazdi MA, Billard A. Outstanding shortening of the activation process stage for a TiFe-based hydrogen storage alloy. Mater Res Bull 2019;112:132–41. https://doi.org/10.1016/j.materresbull.2018.12.015.
[27] Linstrom P. NIST Chemistry WebBook, NIST Standard Reference Database 69. National Institute of Standards and Technology; 1997.
[28] MatWeb. Material Property Data: Mitsui TPX® RT18 Methylpentene Copolymer, Transparent Grade. [April 18, 2024]; Available from: https://www.matweb.com/search/datasheet.aspx?matguid=b0f93692165e4d7fa98087bc874241c4.
[29] Zhu L-F, Friák M, Udyansky A, Ma D, Schlieter A, Kühn U, et al. Ab initio based study of finite-temperature structural, elastic and thermodynamic properties of FeTi. Intermetallics 2014;45:11–7. https://doi.org/10.1016/j.intermet.2013.09.008.
[30] Tjahjono M, Schreyer MK, Guo L, Garland M. Determination of the individual specific heat capacities of solids from multi-component powder mixtures and polymorphic mixtures. J Therm Anal Calorim 2012;108(1):361–70. https://doi.org/10.1007/s10973-011-1928-4.
[31] Mamunya Y, Davydenko VV, Pissis P, Lebedev EV. Electrical and thermal conductivity of polymers filled with metal powders. Eur Polym J 2002;38(9):1887–97. https://doi.org/10.1016/S0014-3057(02)00064-2.
[32] Terada Y, Ohkubo K, Nakagawa K, Mohri T, Suzuki T. Thermal conductivity of B2-type aluminides and titanides. Intermetallics 1995;3(5):347–55. https://doi.org/10.1016/0966-9795(95)94253-B.
[33] Comsol. COMSOL Multiphysics Reference Manual. Version: Comsol 2021;6.
[34] Baehr HD. Heat and Mass Transfer. Berlin, Heidelberg: Springer-Verlag, Berlin Heidelberg; 2006.
[35] Lototsky MV, Davids MW, Fokin VN, Fokina EE, Tarasov BP. Hydrogen-Accumulating Materials Based on Titanium and Iron Alloys (Review). Therm Eng 2024;71(3):264–79. https://doi.org/10.1134/S0040601524030030.
[36] Barale J, Dematteis EM, Capurso G, Neuman B, Deledda S, Rizzi P, et al. TiFe0.85Mn0.05 alloy produced at industrial level for a hydrogen storage plant. Int J Hydrogen Energy 2022;47(69):29866–80. https://doi.org/10.1016/j.ijhydene.2022.06.295.
[37] Zhan L, Zhou P, Xiao X, Cao Z, Piao M, Li Z, et al. Numerical simulation and experimental validation of Ti0.95Zr0.05Mn0.9Cr0.9V0.2 alloy in a metal hydride tank for high-density hydrogen storage. Int J Hydrogen Energy 2022;47(91):38655–70. https://doi.org/10.1016/j.ijhydene.2022.09.043.
[38] Wang H, Yi G, Ye J, Feng X, Li Z, Wang S, et al. Intensification of hydrogen absorption process in metal hydride devices with novel corrugated fins: A validated numerical study. J Alloy Compd 2022;926:166759. https://doi.org/10.1016/j.jallcom.2022.166759.